Low-Temperature Structural Transitions in the Phonon-Glass Thermoelectric Material β-Zn_4Sb_3: Ordering of Zn Interstitials and Defects

Johanna Nylén,[†] Sven Lidin,[†] Magnus Andersson,[‡] Bo Brummerstedt Iversen,[§] Hongxue Liu,[⊥] Nate Newman,[⊥] and Ulrich Häussermann*,[#]

Inorganic Chemistry, Stockholm University, SE-10691 Stockholm, Sweden, Solid State Physics, IMIT, Royal Institute of Technology, KTH Electrum 229, SE-16440 Kista, Sweden, Department of Chemistry, University of Aarhus, DK-8000 Aarhus, Denmark, School of Materials, Arizona State University, P.O. Box 876006, Tempe, Arizona 85287-6006 and Department of Chemistry and Biochemistry, Arizona State University, P.O. Box 871604 Tempe, Arizona 85287-1604

Received October 6, 2006. Revised Manuscript Received November 25, 2006

The low-temperature phase transitions of thermoelectric Zn_4Sb_3 have been characterized using single-crystal X-ray diffraction, electrical resistance, and thermal conductivity measurements. Room-temperature stable, disordered β-Zn_4Sb_3 undergoes a phase transition at 254 K to ordered α-Zn_4Sb_3, which has an ideal composition $Zn_{13}Sb_{10}$. Below 235 K, a second low-temperature phase (α'-Zn_4Sb_3) can be detected. The sequence of phase transitions $\beta-\alpha-\alpha'$ is reversible. The $\alpha-\alpha'$ transformation originates from a slight Zn deficiency with respect to $Zn_{13}Sb_{10}$. The actual composition of Zn_4Sb_3 is $Zn_{13-\delta}Sb_{10}$.

1. Introduction

Thermoelectric materials allow for conversion of thermal energy into electrical energy and may play an important role in the search for alternative energy technologies.[1] The thermoelectric performance is expressed by a dimensionless figure of merit, $ZT = S^2T/(\rho\kappa)$, where S is the thermopower, ρ is the electrical resistivity, κ is the thermal conductivity, and T is the temperature. The presence of interdependent transport properties in ZT makes the discovery of thermoelectric materials extremely challenging. Usually, good thermoelectrics are narrow gap semiconductors, which have to be heavily doped. The latter step adjusts the carrier concentration toward an optimum power factor S^2/ρ.

Recently, β-Zn_4Sb_3 emerged as a compelling p-type thermoelectric with high ZT values in the 400−650 K range.[2] Interestingly, the key to the high thermoelectric performance of β-Zn_4Sb_3 lies in the exceptional thermal conductivity (around 1 W m^{-1} K^{-1} at room temperature and decreasing to 0.7 W m^{-1} K^{-1} at 650 K), which is as low as that for glasslike materials. This unexpected phonon-glass behavior of a crystalline material could be attributed to a high degree of intricate zinc disorder.[3,4] At about 250 K, β-Zn_4Sb_3 transforms into a low-temperature modification.[5,6] Surprisingly, complex structured α-Zn_4Sb_3 appears to be completely ordered with a crystallographic composition of $Zn_{13}Sb_{10}$ ($Zn_{3.9}Sb_3$).[7] According to theoretical calculations, ordered α-Zn_4Sb_3 with the $Zn_{13}Sb_{10}$ composition would feature a narrow band gap of 0.3 eV and a fully occupied valence band.[8]

The nature of the disorder in β-Zn_4Sb_3 and its consequences to thermoelectric properties are still not well understood. Clearly, Zn disorder ensures a low κ, but at the same time, it introduces uncertainties about the actual composition of the phase. Small variations in the Zn content will decisively impact the carrier concentration and thus the power factor. Further structural investigations into the low-temperature disorder−order transition of β-Zn_4Sb_3 may answer this question. From resistivity and heat capacity measurements, Mozharivskyi et al. suggested the occurrence of two consecutive transitions[9] and gave further evidence of an intermediate phase with a narrow temperature stability interval between α and β-Zn_4Sb_3.[10]

* Corresponding author. E-mail: Ulrich.Haussermann@asu.edu.
[†] Stockholm University.
[‡] Royal Institute of Technology.
[§] University of Arhaus.
[⊥] School of Materials, Arizona State University.
[#] Department of Chemistry and Biochemistry, Arizona State University.

(1) Tritt, M. T.; Subramanian, M. A. *MRS Bull.* **2006**, *31*, 188. Nolas, G. S.; Poon, J.; Kanatzidis, M. G. *MRS Bull.* **2006**, *31*, 199.
(2) Caillat, T.; Fleurial, J.-P.; Borshchevsky, A. *J. Chem. Phys. Solids* **1997**, *58*, 1119.
(3) Snyder, G. J.; Christensen, M.; Nishibori, E.; Caillat, T.; Iversen, B. B. *Nat. Mater.* **2004**, *3*, 458.
(4) Cargnoni, F.; Nishibori, E.; Rabiller, P.; Bertini, L.; Snyder, G. J.; Christensen, M.; Gatti, C.; Iversen, B. B. *Chem−Eur. J.* **2004**, *10*, 3861.
(5) Ugai, Y. A.; Marshakova, T. A.; Shevchenko, V. Y.; Demina, N. P. *Izv. Akad. Nauk SSSR, Neorg. Mater.* **1969**, *5*, 1381. Shevchenko, V. Y.; Skriplin, V. A.; Ugai, Y. A.; Marshakova, T. A. *Izv. Akad. Nauk SSSR, Neorg. Mater.* **1968**, *4*, 139.
(6) Souma, T.; Nakamoto, G.; Kurisu, M. *J. Alloys Compd.* **2002**, *340*, 275. Souma, T.; Nakamoto, G.; Kurisu, M.; Kato, K.; Takata, M. *22nd International Conference on Thermoelectrics* **2003**, 282. Nakamoto, G; Akai, N.; Kurisu, M. *J. Alloys Compd.* **2006**, doi:10.1016/j.allcom.2006.07.107.
(7) Nylén, J.; Andersson, M.; Lidin, S.; Häussermann, U. *J. Am. Chem. Soc.* **2004**, *126*, 16306.
(8) Mikhailushkin, A. S.; Nylén, J.; Häussermann, U. *Chem.−Eur. J.* **2005**, *11*, 4912.
(9) Mozharivskyj, Y.; Pecharsky, A. O.; Bud'ko, S.; Miller, G. J. *Chem. Mater.* **2004**, *16*, 1580.
(10) Mozharivskyj, Y.; Janssen, Y.; Harringa, J. L.; Kracher, A.; Tsokol, A. O.; Miller, G. J. *Chem. Mater.* **2006**, *18*, 822.

10.1021/cm062384j CCC: $37.00
Published on Web 01/06/2007

In this work, we present a conclusive picture of the low-temperature structural behavior of Zn_4Sb_3. In particular, we show that α-Zn_4Sb_3 actually corresponds to an intermediate, still partially disordered phase, which is succeeded by a closely related and more ordered phase (in the following denoted as α′-Zn_4Sb_3) below 235 K. The occurrence of α′-Zn_4Sb_3 is coupled to a slight Zn deficiency (δ) with respect to the ideal composition $Zn_{13}Sb_{10}$ ($Zn_{13-\delta}Sb_{10}$) and δ in turn becomes a decisive factor for controlling the thermoelectric performance of Zn_4Sb_3.

2. Experimental Section

Zn_4Sb_3 was prepared from a 4:3 Zn:Sb reaction mixture that was pressed into a pellet and heated to 923 K in an evacuated quartz tube. The sample was slowly cooled (at a rate of 5 K/h) to 723 K and subsequently quenched in water. The product was obtained as shiny ingots that were analyzed by X-ray powder diffraction (Guinier camera, Cu $K\alpha_1$) and energy-dispersive X-ray spectroscopy in a JEOL 820 scanning electron microscope. It corresponded to single phase β-Zn_4Sb_3 with an average Zn content of 56.1(4) at %. A single crystal for X-ray diffraction experiments was selected from a crushed ingot and diffraction data was collected on an Oxford diffraction Excalibur 3 system at different temperatures. Resistivity measurements were performed on a bar-shaped fragment of a crushed ingot ($1 \times 1.5 \times 4$ mm^3) using a four-point in-line contact arrangement. Thermal conductivity was measured on a polished piece of ingot ($2 \times 2 \times 7$ mm^3) with a Quantum Design physical property measurement system (PPMS).

3. Results and Discussion

Single-crystal diffraction data were collected at the temperatures 250, 245, 240, 235, 230, 200, and 120 K. Selected results are displayed in Figure 1a, showing the peculiar structural evolution of Zn_4Sb_3 with decreasing temperature. The patterns taken at 250 and 245 K correspond to rhombohedral β-Zn_4Sb_3 (space group $R\bar{3}c$; $a \approx 12.2$ Å, $c \approx 12.4$ Å), which contains three distinct atomic positions (36f Zn, 18e Sb1, and 12c Sb2).[11] Accordingly, the composition would be Zn_6Sb_5. However, Zn disorder in β-Zn_4Sb_3 manifests in interstitial Zn atoms distributed on three weakly occupied general sites 36f. Additionally, the regular Zn position displays a considerable occupational deficiency (0.89−0.9). The composition obtained from the refined occupancies of the different Zn sites is $Zn_{3.83}Sb_3$.[3,4]

A transition to the (twinned) α-phase occurs between 245 and 240 K. The reflections characteristic for this phase quadruple the rhombohedral $[\bar{1}01]^*$ direction (hexagonal setting), allowing for six distinct domain orientations corresponding to the 3-fold rotational symmetry and the c-glide of the original $R\bar{3}c$ symmetry. The structure is centrosymmetric with triclinic symmetry, but has a metrically C-centered monoclinic unit cell ($C\bar{1}$; $a \approx 32.5$ Å, $b \approx 12.2$ Å, $c \approx 10.9$ Å, $\beta \approx 99°$).[7] The two Sb positions in β-Zn_4Sb_3 split into 20 independent positions, whereas Zn occupies 26 independent positions. The ideal composition of this phase amounts to $Zn_{13}Sb_{10}$ ($Zn_{3.9}Sb_3$). However, it is difficult to ascertain full occupancy of the Zn positions because of the combination of a high degree of pseudo-symmetry and twinning.

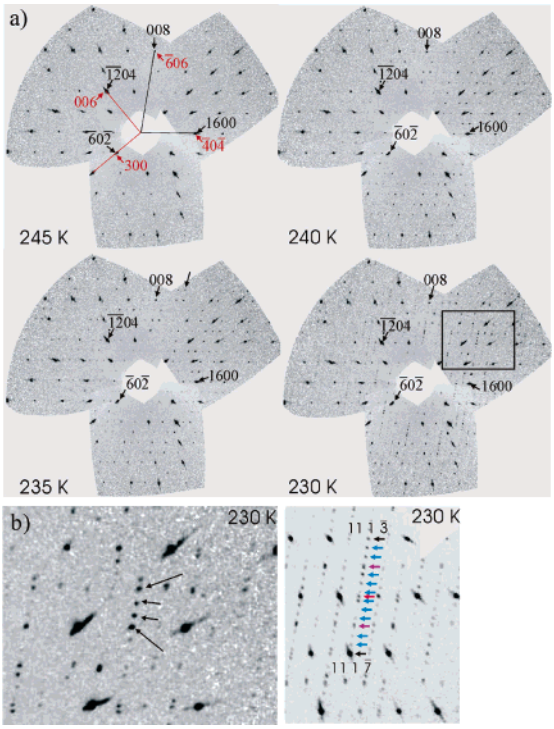

Figure 1. X-ray diffraction patterns for Zn_4Sb_3 at different temperatures along the hexagonal [010]* direction. Hexagonal axes and indices (β-Zn_4Sb_3) are shown in red and the monoclinic counterparts (α-Zn_4Sb_3) are shown in black. At 240 K, the superstructure reflections of the α phase appear and are fully expressed at 235 K (leading to a quadrupling of the $[\bar{1}01]^*_{hex}$ direction, which is the monoclinic c^* direction). At 230 K, satellites of the α′-Zn_4Sb_3 structure emerge. They appear very close to tripling the α-phase superstructure reflections. (b) Detailed diffraction patterns obtained at 230 K. The left-hand side corresponds to an enlarged presentation of the section marked in (a) showing α phase superstructure reflections with long and α′ satellites with short arrows. The right-hand side shows a section of the (*h*1*l*) reciprocal plane. Black arrows point at basis structure reflections. Blue and purple arrows point at reflections belonging to the 13-fold superstructure from the α′ phase. Purple and red arrows point at reflections from the remaining α phase. Note the overlapping reflections from α and α′ (purple arrows).

From 230 K and below, the diffraction pattern becomes much more complex (Figure 1b). New satellites that are clearly incommensurate with the 4-fold super structure emerge. A high-resolution dataset (0.3° scan width) at 120 K conclusively shows that the new satellites coexist with the α-phase, but form a set that is disjoint from the α-phase **q**-vectors. The α′ satellites run in directions parallel to those of the α-phase, $[\bar{1}01]^*_{hex}$, but the **q**-vector is of the form $1/13(\bar{1}01)^*$ rather than $1/4(\bar{1}01)^*$, and there are no cross-terms between the two sets. The most likely explanation is that the α′-phase coexists with the α-phase. Judging from the intensity of the satellite reflections, the same domain orientation dominates for the α′-phase as for the α-phase. Interestingly, this behavior is reproducible. Temperature cycling results in the same predominant domain orientation for both the α- and the α′-phases.

The structure of the α-phase is strikingly similar to that of the β-phase (for a detailed discussion, see ref 8). Their common feature is planar rhomboid rings Zn_2Sb_2 with a short Zn-Zn contact (2.8 Å) that are condensed into chains by

(11) Mayer, H. W.; Mikhail, I.; Schubert, K. *J. Less-Common Met.* **1978**, *59*, 43.

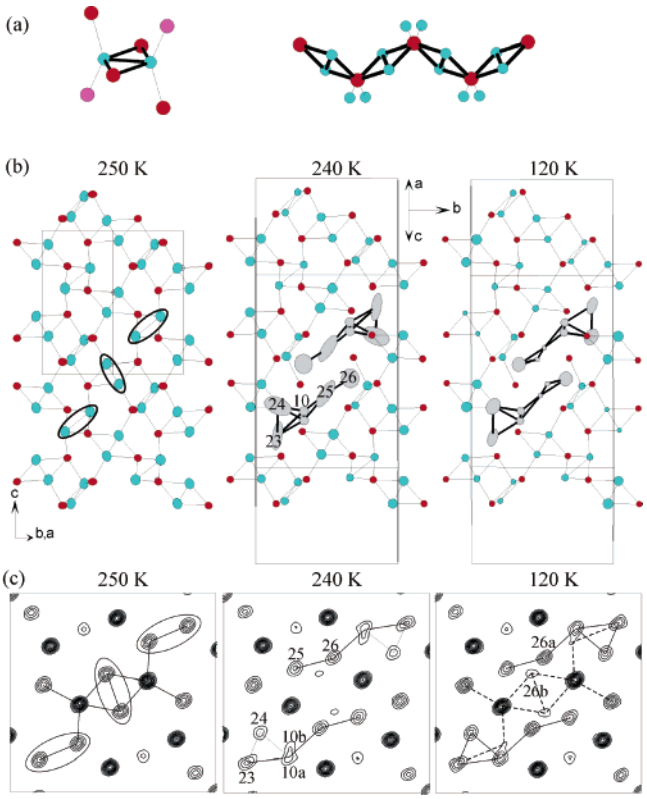

Figure 2. (a) Building unit of the structures of α and β-Zn_4Sb_3. Green circles denote Zn atoms, red and purple circles denote the two different types of Sb atoms. Rhomboid rings Zn_2Sb_2 (emphasized with bold lines) are condensed into chains, which run in three different directions and are connected by Zn-Sb1 and Zn-Sb2 bonds. (b) Equivalent sections of β-Zn_4Sb_3 (250 K), α-Zn_4Sb_3 (240 K), and α′-Zn_4Sb_3 (120 K). Sb2 atoms are omitted for clarity. Regular (rhombohedral) Zn atoms are drawn as green and interstitial Zn atoms (arranged as five-atom clusters) as gray ellipsoids (99% probability). In the section of β-Zn_4Sb_3 the pairs of regular Zn atoms becoming vacancies in α-Zn_4Sb_3 are high-lighted. (c) Corresponding Fourier maps to (b) showing the origin of the split positions (summation over a 2 Å layer); interstitial clusters are partially replaced by regular Zn atoms.

sharing common Sb atoms (Figure 2a). These chains run in three different directions and are linked by Zn−Sb bonds. The Sb atom substructures of α and β-Zn_4Sb_3 differ only fractionally and also large parts of the Zn atom substructure are virtually identical in both structures. Twenty-one out of the 26 Zn positions in α-Zn_4Sb_3 correspond to regular framework Zn atoms (pairs) within the rhomboid rings in β-Zn_4Sb_3. The remaining five positions ("non-rhombohedral" Zn atoms, denoted as Zn10, Zn23, Zn24, Zn25, and Zn26) are then associated with the interstitial Zn atoms in disordered β-Zn_4Sb_3. These atoms are assembled in clusters consisting of a triangle with a tail of two more Zn atoms attached. Two five-atom clusters are grouped together and related by a center of inversion. Each pair of five-atom clusters replaces three pairs of Zn atoms from the regular rhomboid ring framework in β-Zn_4Sb_3 (Figure 2b). These missing pairs of Zn atoms are associated with the vacancies in β-Zn_4Sb_3.

Structural refinements of the datasets measured below the α−β transition were initiated using the model of the α-phase.[7,12] Because the Sb atoms are only weakly affected by the superstructure ordering, they were constrained so that the Sb atoms corresponding to the 18e and 12c positions of

(12) Petricek, V.; Dusek, M. *The Crystallographic Computing System JANA2000*; Institute of Physics: Praha, Czech Republic, 2000.

Table 1. Lattice Parameters and Refinement *R* Factors for the α-Zn_4Sb_3 Structure at 120 and 240 K

T (K)	*a* (Å)	*b* (Å)	*c* (Å)	α (deg)	β (deg)	γ (deg)	R_{obs}[a]
240	32.620(3)	12.243(2)	10.887(1)	89.95(1)	99.05(1)	89.93(1)	4.68
120	32.546(3)	12.237(2)	10.874(2)	90.00(1)	99.01(1)	89.67(1)	5.25

[a] Weighting scheme $w = 1/(\sigma^2(F)+0.0016F^2$, observed threshold $F > 3\sigma(F)$.

Table 2. Refined Positional Parameters for Interstitial Zn Atoms in the Structure of α-Zn_4Sb_3 at 240 and 120 K (for remaining parameters, see ref 7)

atom	occupancy	*x*	*y*	*z*	U_{iso} (Å^2)
		T = 240 K			
Zn10b	0.432(7)	0.3897(3)	0.6611(8)	0.5776(8)	0.023(1)
Zn23b	0.390(1)	0.1413(3)	0.6589(9)	0.320(1)	0.022(1)
Zn26b	0.330(6)	0.4566(4)	0.459(1)	0.485(1)	0.025(1)
Zn10a	0.568(7)	0.3630(2)	0.6596(6)	0.6029(6)	0.023(1)
Zn23a	0.610(7)	0.1473(2)	0.6499(5)	0.2434(6)	0.022(1)
Zn24	0.64(1)	0.0881(2)	0.6570(5)	0.4026(5)	0.029(2)
Zn25	0.73(1)	0.4485(2)	0.3346(5)	0.4195(5)	0.039(2)
Zn26a	0.670(6)	0.4257(2)	0.5140(5)	0.5272(5)	0.025(1)
		T = 120 K			
Zn10b	0.270(8)	0.3907(5)	0.653(1)	0.585(1)	0.020(1)
Zn23b	0.245(8)	0.1415(5)	0.662(1)	0.308(2)	0.018(1)
Zn26b	0.283(6)	0.4570(4)	0.460(1)	0.494(1)	0.009(1)
Zn10a	0.730(8)	0.3633(2)	0.6591(5)	0.6036(4)	0.020(1)
Zn23a	0.755(8)	0.1473(2)	0.6494(4)	0.2409(5)	0.018(1)
Zn24	0.71(1)	0.0886(2)	0.6550(4)	0.4019(4)	0.013(2)
Zn25	0.71(1)	0.4486(2)	0.3342(4)	0.4223(4)	0.010(2)
Zn26a	0.717(6)	0.4254(1)	0.5141(4)	0.5272(4)	0.009(1)

the rhombohedral phase were modeled using one isotropic displacement parameter, respectively. All Zn positions corresponding to regular framework atoms were treated using isotropic displacement parameters, whereas interstitial atoms were treated anisotropically. Because of the coexistence of the α and α′ phase below the α−α′ transition, it was possible to integrate intensities corresponding to the α-phase even at the lowest temperatures measured, although the effect of overlapping reflections is difficult to estimate. The refinement results are compiled in panels b and c of Figure 2 and in Tables 1 and 2. Not surprisingly, the interstitial Zn atoms show a large anisotropy, and it turned out that it was in fact not possible to model the behavior of the position Zn10 using anisotropy, but a split position had to be introduced. For the measurement at 120 K, the atom Zn26 also required a split position description.

A close inspection of equivalently obtained Fourier maps at different temperatures revealed a striking explanation for these split positions (Figure 2c). Zn10b and Zn26b correspond to regular, i.e., "rhombohedral", framework Zn positions in β-Zn_4Sb_3. This indicates a scenario where the α-phase is somewhat poor in Zn with respect to the ideal 13:10 composition. Interstitial Zn sites forming five-atom clusters are then not completely occupied, but partly replaced by pairs of Zn atoms of the regular framework. Subsequently, Zn23 was also treated as split position. In the final refinements, Zn23b−Zn10b−Zn26b account for a vacancy free framework with a composition $Zn_{12}Sb_{10}$ and Zn23a−Zn24−Zn10a−Zn25−Zn26a for the ideal α-Zn_4Sb_3 (ordered interstitials/vacancies) structure with composition $Zn_{13}Sb_{10}$. The site occupancies for Zn23b−Zn10b−Zn26b (group I) and Zn23a−Zn24−Zn10a−Zn25−Zn26a (group II) are clearly correlated. Within each group, values are very similar (∼0.3 and ∼0.7, respectively), which suggests that interstitial

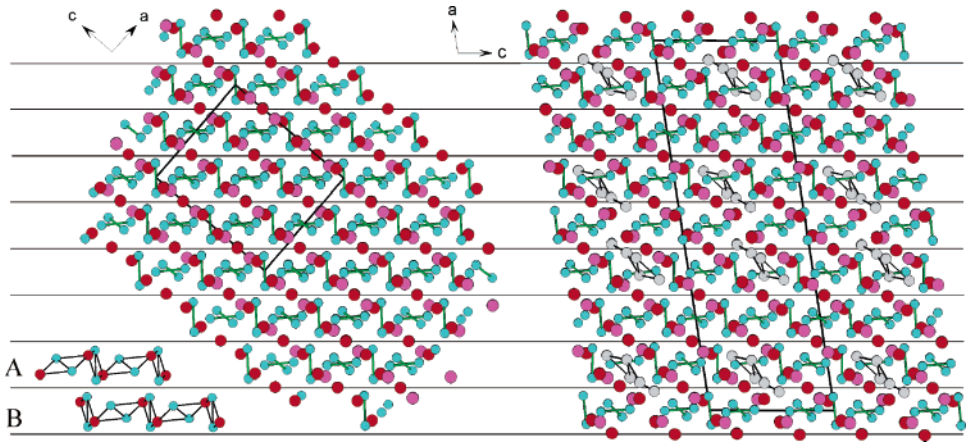

Figure 3. Rhombohedral $Zn_{12}Sb_{10}$ framework (left) and the structure of triclinic α-Zn_4Sb_3 (right-hand side) viewed along [010]. The color code is as in Figure 2. Bonds are drawn between short Zn contacts within interstitial clusters and rhomboid rings Zn_2Sb_2. The projection allows us to compare the $Zn_{12}Sb_{10}$ framework and α-Zn_4Sb_3 structure in terms of layers (solid horizontal lines) composed of parallel chains of Zn_2Sb_2 rings (lower left corner) running in two different directions (*A* and *B*). In α-Zn_4Sb_3, pairs of interstitial five-atom Zn clusters (gray) are hosted in blocks consisting of three consecutive layers (*ABA*), which are separated by an empty, interstitial-free layer (*B*). This gives rise to a quadrupling along the stacking direction of the layers. A pair of interstitial five-atom Zn clusters replaces three pairs of Zn atoms from rhomboid rings of the regular framework (green).

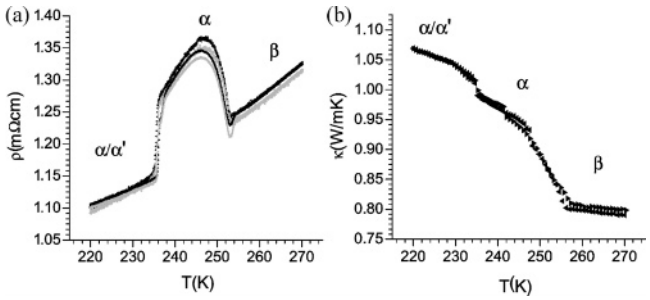

Figure 4. Physical property changes of Zn_4Sb_3 along the sequence of phase transitions $\beta-\alpha-\alpha'/\alpha$. (a) Electrical resistivity ρ, (b) thermal conductivity κ. Two cooling and heating cycles were performed for ρ (distinguished by black and gray symbols, respectively) and one for κ.

clusters maintain their integrity upon Zn deficiency in α-Zn_4Sb_3. From the refined site occupancies, α-Zn_4Sb_3 has a composition of $Zn_{12.69(1)}Sb_{10}$ at 240 K and $Zn_{12.71(1)}Sb_{10}$ at 120 K.

To understand the occurrence of α′-Zn_4Sb_3 exhibiting further superstructure ordering, we have to recall the peculiar $[\bar{1}01]^*_{hex}$ or monoclinic c^* direction as the direction of the **q**-vectors for both the α and α′ phase. Figure 3 shows relevant projections of the crystal structures of the disorder-free rhombohedral $Zn_{12}Sb_{10}$ framework and ideal α-Zn_4Sb_3. Interestingly, in the [010] projection, $Zn_{12}Sb_{10}$ emerges as being composed of layers defined by chains of rhomboid rings Zn_2Sb_2 (cf. Figure 2a) running parallel. In consecutive layers, two different chain directions alternate, yielding an *AB*-like stacking. In α-Zn_4Sb_3, pairs of interstitial five-atom Zn clusters are hosted in *ABA* blocks of such layers, which are separated by an empty, interstitial-free layer (*B*). This gives rise to quadrupling along the stacking direction of the layers. Zn deficiency can now be expressed as missing interstitial clusters within a block and/or the insertion of additional interstitial-free layers between *ABA* blocks. In the α-phase occurring in the intermediate temperature range, this Zn deficiency is randomly distributed and an attractive idea is to assume both types of disorder. The two-phase diffraction patterns below 235 K can then be explained by an ordering of the layer-type Zn deficiency, which is accompanied by a disproportionation into α′-Zn_4Sb_3 with a 13 layer stacking sequence (e.g., one additional interstitial-free layer per three blocks *ABAB*) and α-Zn_4Sb_3 without any layer-type Zn deficiency. The two phases would have slightly different compositions, and with respect to the intermediate temperature α-phase, α′ would be comparatively poor in Zn and low temperature α richer. The ultimate proof of this hypothesis rests in the structural solution and refinement of α′-Zn_4Sb_3, which is, however, hampered by the difficulty in generating useful intensities because reflections are very closely spaced and overlap severely with those of the α-phase (cf. Figure 1b).

The sequence of transitions $\beta-\alpha-\alpha'/\alpha$ observed in the diffraction experiment is also clearly visible in electrical resistivity measurements, where several cooling and heating cycles were carried out at slow rate (0.2−0.5 K/min). Upon cooling, the $\beta-\alpha$ transition occurs at 253−254 K, and upon heating, the $\alpha'/\alpha-\alpha$ transition takes place at 233−235 K. For both transitions, hysteresis during cycling is very small. We note that these transition temperatures match well with the observation from the single-crystal diffraction study ($\beta-\alpha$ between 245 and 250 K, and $\alpha-\alpha'/\alpha$ between 230 and 235 K; note that the temperature uncertainty in low-temperature single-crystal diffraction experiments is much larger compared to physical property measurements).

Concerning the low-temperature behavior of the thermal conductivity κ, we recall that the peculiarity of Zn_4Sb_3 is exceptionally low κ values in the 300−650 K range due to the disordered zinc in β-Zn_4Sb_3. The room-temperature value of our sample is 0.8 W K^{-1} m^{-1}, which is somewhat lower than the value reported by Caillat et al.[2] Upon cooling, κ remains virtually constant until the $\beta-\alpha$ transition. In the temperature region of intermediate α-Zn_4Sb_3, κ increases to about 1 W K^{-1} m^{-1}. At 235 K, the $\alpha-\alpha'/\alpha$ transition can be recognized in a slight discontinuous rise of κ. Interestingly, the transition from the disordered β phase to increasingly higher ordered α and α′/α-Zn_4Sb_3 with much larger unit-cell structures than β-Zn_4Sb_3 has a pronounced effect on κ, but does not lead to dramatically increased values.

In conclusion, we find that the state-of-the-art thermoelectric material β-Zn_4Sb_3 undergoes a sequence of low-

temperature transitions $\beta-\alpha-\alpha'/\alpha$,which is observed reversibly in a single-crystal diffraction experiment and physical property measurements. During the $\beta \rightarrow \alpha$ transformation, randomly disordered zinc interstitials and vacancies order into islands consisting of three vacant pairs of regular Zn atoms and one pair of five-atom clusters of interstitial Zn atoms. The $\alpha \rightarrow \alpha'/\alpha$ transition is triggered by not completely occupied ordered interstitial Zn positions, and the resulting occupational modulation can be interpreted as a further step of ordering. As a consequence, the composition of Zn_4Sb_3 has to be rephrased as $Zn_{13-\delta}Sb_{10}$. This was already indicated in the initial refinements of the disordered β-phase by Snyder et al. and Cargnoni et al., who obtained a significant deviation from the ideal composition (i.e., $Zn_{3.83}Sb_3$, corresponding to $\delta = 0.23$),[3,4] and is now put on a firm ground by the refinement of the crystallographically much better described intermediate α-phase, which has the same composition as β-Zn_4Sb_3. For our sample, δ is around 0.3. At this stage, it is not clear what the maximum value of δ is or if samples with $\delta = 0$ can actually be synthesized. However, Zn deficiency with respect to the composition $Zn_{13}Sb_{10}$, which yields a completely filled valence band for α-Zn_4Sb_3,[8] must have a chief implication to the charge carrier (hole) concentration in p-type Zn_4Sb_3. A slightly variably δ for differently prepared Zn_4Sb_3 samples would explain the rather large scattering of measured resistivity and thermopower values for this material. Reported room temperature ρ values range from 0.8 to 3.3 mΩ cm and S values from 70 to 142 μV/K.[2,6,13] The challenge lies now in the optimization of the power factor S^2/ρ of Zn_4Sb_3 by controlling δ through special synthesis and doping methods.

Acknowledgment. This work was supported by the Swedish Research Council (VR).

CM062384J

(13) Kim, I.-H.; Park, J.-B.; Hong, T.-W.; Ur, S.-C.; Lee, Y.-G.; Ryu, S.-L.; Nakamoto, G.; Kurisu, M. *Mater. Sci. Forum* **2006**, *510*−511, 1070. Nakamoto, G.; Souma, T.; Yamaba, M.; Kurisu, M. *J. Alloys Compd.* **2004**, *377*, 59. Ur, S.-C.; Nash, P.; Kim, I.-H. *J. Alloys Compd.* **2003**, *361*, 84. Ur, S.-C.; Kim, I.-H.; Nash, P. *Mater. Lett.* **2004**, *58*, 2132. Ur, S.-C.; Nash, P.; Kim, I.-H. *Mater. Lett.* **2004**, *58*, 2937.